

SAE Technical Paper Series

850523

Silicon Nitride Swirl Lower-Chamber for High Power Turbocharged Diesel Engines

Sumio Kamiya,
Mikio Murachi,
Hiroshi Kawamoto,
Satoshi Kato,
Seiho Kawakami
and Yasumitsu Suzuki

Toyota Motor Corp.

International Congress
& Exposition
Detroit, Michigan
February 25 – March 1, 1985

The appearance of the code at the bottom of the first page of this paper indicates SAE's consent that copies of the paper may be made for personal or internal use, or for the personal or internal use of specific clients. This consent is given on the condition, however, that the copier pay the stated per article copy fee through the Copyright Clearance Center, Inc., Operations Center, P.O. Box 765, Schenectady, N.Y. 12301, for copying beyond that permitted by Sections 107 or 108 of the U.S. Copyright Law. This consent does not extend to other kinds of copying such as copying for general distribution, for advertising or promotional purposes, for creating new collective works, or for resale.

Papers published prior to 1978 may also be copied at a per paper fee of \$2.50 under the above stated conditions.

SAE routinely stocks printed papers for a period of three years following date of publication. Direct your orders to SAE Order Department.

To obtain quantity reprint rates, permission to reprint a technical paper or permission to use copyrighted SAE publications in other works, contact the SAE Publications Division.

ISSN 0148-7191

Copyright © 1985 Society of Automotive Engineers, Inc.

This paper is subject to revision. Statements and opinions advanced in papers or discussion are the author's and are his responsibility, not SAE's; however, the paper has been edited by SAE for uniform styling and format. Discussion will be printed with the paper if it is published in SAE Transactions. For permission to publish this paper in full or in part, contact the SAE Publications Division.

Persons wishing to submit papers to be considered for presentation or publication through SAE should send the manuscript or a 300 word abstract of a proposed manuscript to: Secretary, Engineering Activity Board, SAE.

Printed in U.S.A.

850523

Silicon Nitride Swirl Lower-Chamber for High Power Turbocharged Diesel Engines

Sumio Kamiya,
Mikio Murachi,
Hiroshi Kawamoto,
Satoshi Kato,
Seiho Kawakami
and Yasumitsu Suzuki

Toyota Motor Corp.

ABSTRACT

This paper describes application of sintered silicon nitride to the swirl lower-chamber in order to improve performance of turbocharged diesel engines. Various stress analyses by finite element method and stress measurements have been applied to determine the design specifications for the component, which compromise brittleness of ceramic materials. Material development was conducted to evaluate strength, fracture toughness, and thermal properties for the sintered bodies. Ceramic injection molding has been employed to fabricate components with large quantities in the present work. Quality assurance for the components can be made by reliability evaluation methods as well as non-destructive and stress loading inspections. It is found that the engine performance with ceramic component has been increased in the power out put of 9PS as compared to that of conventional engines.

SILICON NITRIDE SINTERED MATERIAL has potential for high performance applications for gas turbine engines or automotive engines because of its high temperature capabilities, wear resistance and resistance to chemical attack. It is expected to make engine performance improve by application of sintered silicon nitride to the combustion systems for diesel engines, since an increase in temperature for engine operation will be possible. New techniques must be developed to succeed in application of ceramic component to automotive engineerings.

In this paper, several techniques will be discussed which are essential for development of ceramic swirl lower-chamber, including design methods, material evaluations, fabrication process, inspection methods and reliability evaluation methods.

ENGINE PERFORMANCE OBJECTIVE

The engine employed in this work is 2L-THE electronic controlled turbocharged diesel engine carried on "TOYOTA CROWN". A cross section of this engine is shown in Fig.1. Maximum power out put can be increased by increasing in the temperature of combustion chamber as shown in Fig.2. The temperature was measured by inserting a thermocouple into top end of the glow plug. The inside surface temperature of swirl lower-chamber can be estimated to be $\approx 100^{\circ}\text{C}$ lower than that of combustion chamber. The maximum operation temperature is limited to $\approx 930^{\circ}\text{C}$ in the case of ordinary metal chamber, since it may be cracked due to strength degradation above this temperatures.

In this work, the objective of the maximum temperature of combustion chamber is determined to be 970°C by use of ceramic swirl chamber, where engine performance in power will be expected to be increased from 96 to 105PS of the order of top class as shown in Fig.3.

PROBLEMS IN DEVELOPMENT

Sintered silicon nitride is high performance structural material, but this material has disadvantages for its brittleness and large strength variations. This is attributed to the fact that the strength of ceramic materials depends on surface flaws or internal defects. Figure 4 shows typical example for failed component after engine durability testing in early stage of this development. Therefore, it is necessary to approach from view points of both material evaluations and design methods so as to employ ceramic component in engine applications.

Design methods must be considered to compromise brittleness of ceramic materials. Fabrication process is required to improve strength, to reduce strength variations, and to minimize defects. Moreover, it is essential to

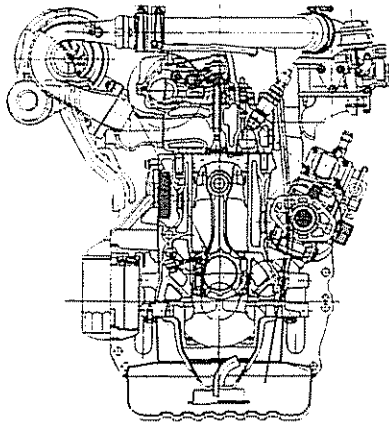


Fig. 1 - Cross section of engine employed in the present work

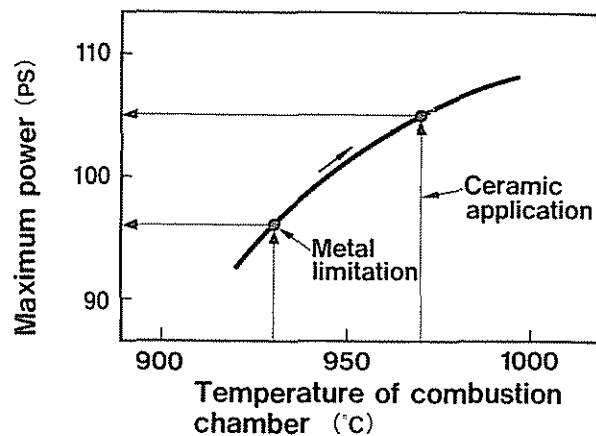


Fig. 2 - Conceptual illustration for maximum power out put

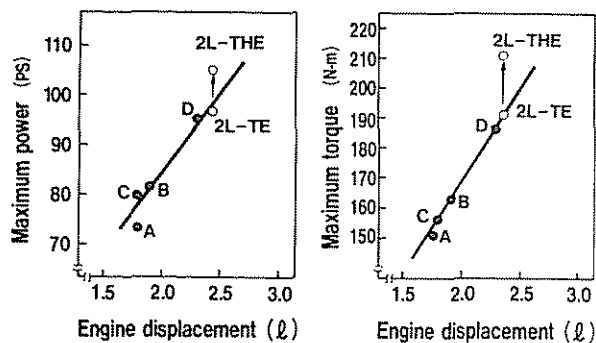


Fig. 3 - The objective and comparison of engine performance

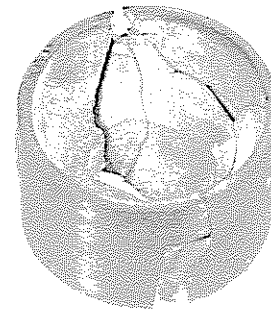


Fig. 4 - Failed ceramic swirl lower-chamber

ensure component reliability by several inspections and reliability evaluations that are suitable for ceramic materials.

The development for these techniques will be discussed below.

COMPONENT DESIGN METHODS

The shape of ceramic chamber is similar to ordinary one of Ricardo Comet MK-V type (Fig.5). This shape has advantages for good performance and noise characteristics. External surface is straight type to reduce stress concentration. Service stresses applied to the swirl chamber can be generated by mainly thermal stress and combustion stress. Other stresses are associated with fixing forces from cylinder head gasket or the forces generated by thermal deformation of cylinder head. The model for these stresses is illustrated in Fig.6.

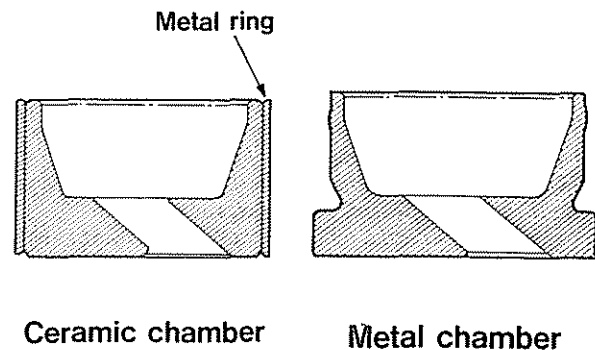


Fig. 5 - Comparison of the shape of swirl lower-chamber

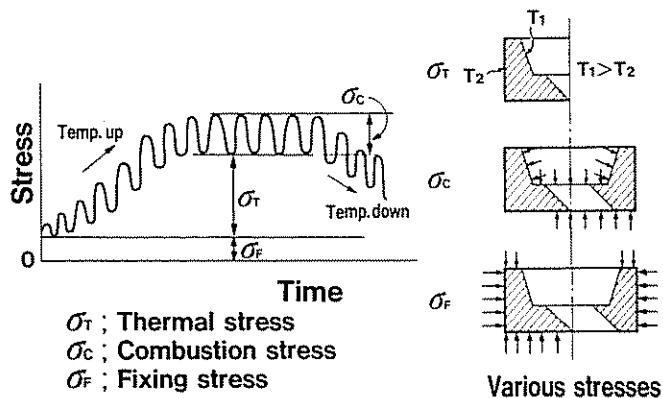


Fig. 6 - The model for service stresses

STRESS ANALYSIS BY FINITE ELEMENT METHOD- Figure 7 shows three dimensional solid model for FEM analysis in ceramic swirl chamber. Temperature distribution was analyzed by FEM, which was based on the results for temperature measurement in the component under engine operation (Fig.8). The temperature of inside surface of the chamber becomes lower than that of combustion chamber because of the existence of boundary layer in periphery of the component. However, it can be recognized that there exists relatively large temperature gradient towards external surface of the swirl chamber. Figure 9 shows distribution of thermal stress calculated by above results. Large thermal stresses can be generated in the upper and lower out side as well as throat region in the component. Maximum stress was estimated to be $\approx 290\text{MPa}$ as tensile stress.

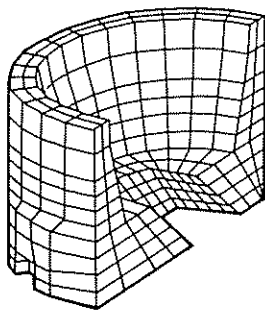


Fig. 7 - Three dimensional solid model for FEM

The service stresses were also measured using strain gages under engine operation. The result is shown in Fig.10. It is apparent that the stresses are increased according to an increase in engine speed, and the swirl chamber is subject to dynamic stresses. The ultimate stresses were estimated by the combination of above measured stresses and FEM analysis, as it is difficult to measure the ultimate stress distribution due to temperature limit for strain gages.

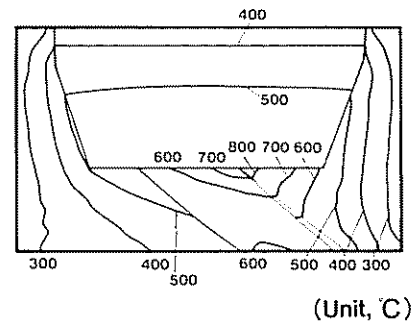


Fig. 8 - Temperature distribution calculated by FEM

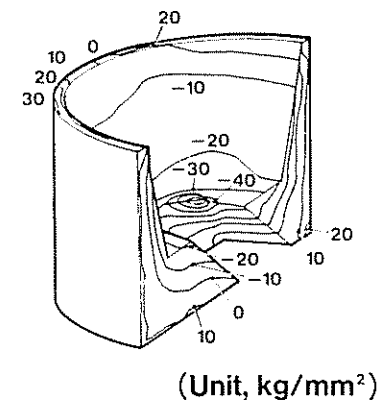


Fig. 9 - Thermal stress distribution calculated by FEM

The present swirl chamber is designed to install the outer metal ring of shrink-fit to reduce stresses applied to upper and lower regions. Figure 11 shows FEM stress analysis to determine the shrink-fit clearance as well as the thickness for upper region of the chamber. Relatively large shrink-fit clearance and small thickness are favorable to reduce applied stresses. Optimum values for them were determined by above FEM analysis followed by engine durability confirmation.

STRESS ANALYSIS FOR FIXING FORCE -

Figure 12 shows deformation pattern for a cylinder head by temperature gradient, where the head is deformed elliptically by compressive stress. This is consistent with the result obtained by strain measurement under engine operation. The clearance (A) in Fig.13 is necessary to reduce stress generated by such a cylinder head deformation.

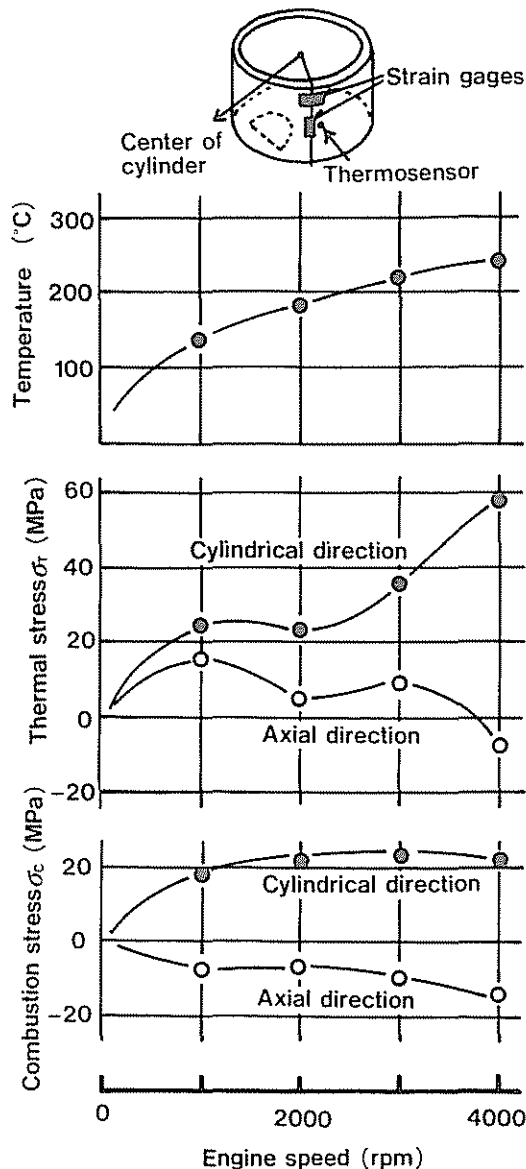


Fig.10 - Measured service stresses applied to swirl lower-chamber

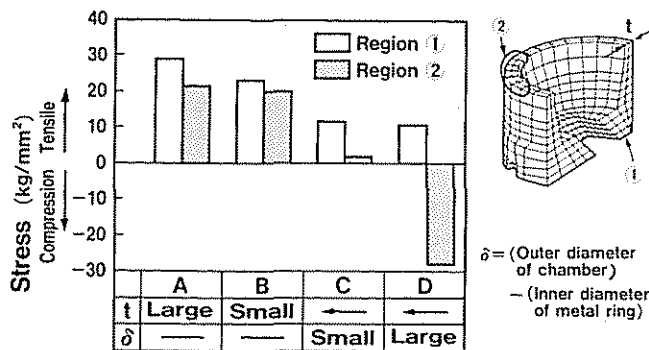


Fig.11 - FEM stress analysis for determination for thickness and shrink-fit clearance

Other stress must be considered which is due to the force from cylinder head gasket. The clearance (B) between bottom surface of the chamber and lower end of the cylinder head is particularly important (Fig.13). Figure 14 shows the correlation between this clearance and stresses applied to the external surface of the chamber. It can be seen that the stresses tend to decrease according to an increase in this clearance.

It is necessary to minimize the stresses due to these fixing forces as for initial stress.

STRESS ANALYSIS FOR A FITTING HOLE IN THE CHAMBER - The fitting pin prevents from rotating the swirl chamber as well as making it loose into the cylinder head. Figure 15 shows FEM analysis for stress distribution around the fitting hole in bottom surface of the chamber. The result indicates that stress concentration is assumed to be not serious problem, because higher stress can be generated besides the fitting hole.

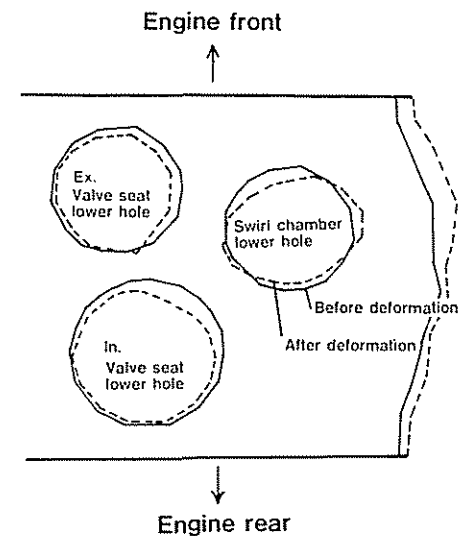


Fig.12 - Deformation pattern of cylinder head

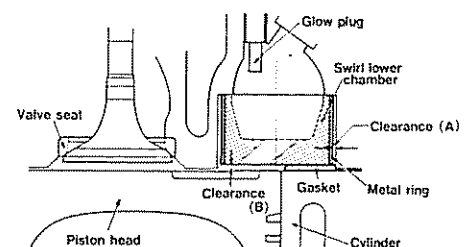


Fig.13 - Assembling for swirl lower-chamber

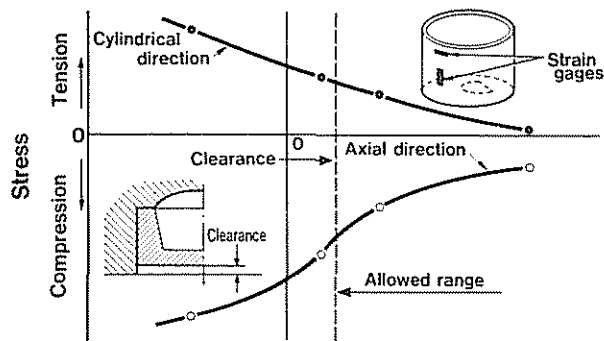


Fig.14 - Clearance and applied stresses in external surface of swirl lower-chamber

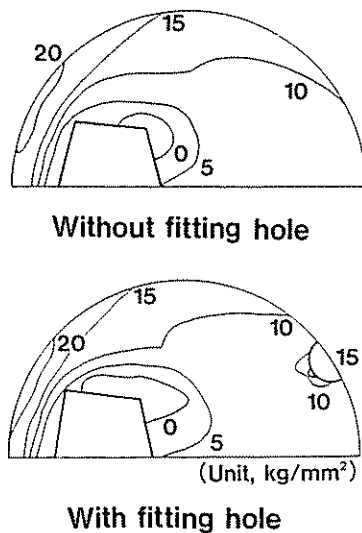


Fig.15 - FEM stress analysis in bottom surface of swirl lower-chamber

FABRICATION PROCESS

MATERIAL DEVELOPMENT - Silicon nitride powder has average particle size of 0.8~0.9 μ m, and α -Si₃N₄ content is more than 90%. Yttrium oxide and spinel were used as for sintering additives. Silicon nitride were mixed with oxide additives in ball mill under ethanol. Testing bars were molded in die by pressing followed by cold isostatic pressing. The testing bars were machined to final size of 3 X 4 X 32mm after sintering for 4hrs at 1750°C under N₂ ambient. Flexural strength by three point bending were measured by span 30mm and cross-head speed of 0.5mm/min at room temperature. Flexural strength of sintered material has 715Mpa with Weibull parameter of 18.7 as shown in Fig.16. Microstructure for the sintered body is composed of fine crystalline particles with the order of between submicron and a few microns. The rectangular crystallines are also observed in Fig.17.

The properties of sintered material can be affected by the amount of oxide additives. Flexural strength has slightly increased from 715 to 745MPa according to decrease in additives from 5-5 to 4-4w/o. Small amount of additives is favorable to improve high temperature properties as glass phase can be decreased, but relative density was low in the case of less additives than 4-4w/o in the present work. Hence, it was concluded that the oxide additives was sufficient to 4-4w/o.

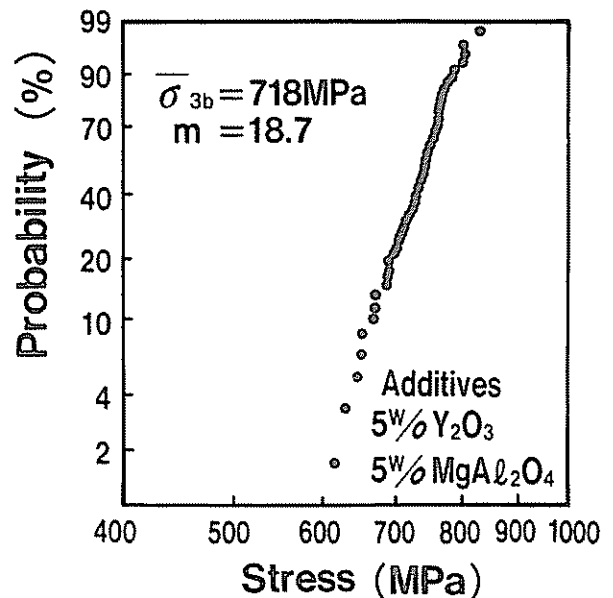


Fig.16 - Flexural strength at room temperature

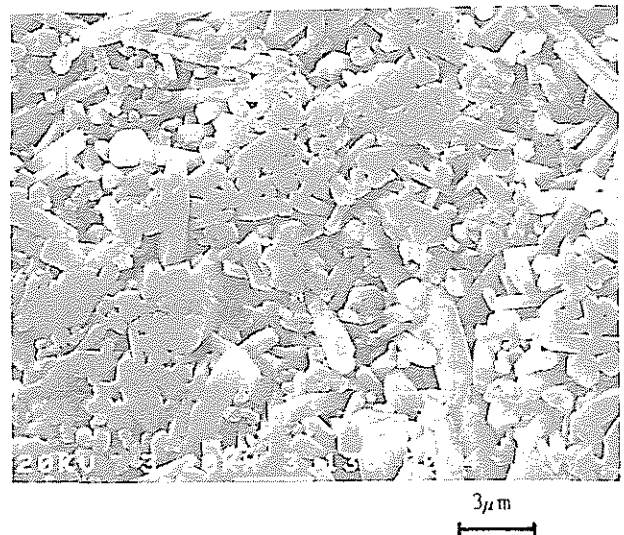


Fig.17 - Micro-structure of etching surface of sintered body

Thermal properties of sintered body are summarized in Table 1. Thermal conductivity can be increased according to decrease in additives, which is presumably due to thermal scattering effect of glass phase. Increase in thermal conductivity is advantageous for reduction of thermal stress applied to the swirl chamber.

Table 1 - Thermal properties of sintered body in the present work

Temp. (°C)	Additives (W%)	Thermal diffu. coefficient (m ² /s)	Specific heat capacity (KJ/kg·k)	Thermal conductivity (W/m·k)
20	5-5	8.164×10^{-6}	0.6737	17.75
	4-4	9.275×10^{-6}	0.6904	20.60
590	5-5	3.66×10^{-6}	0.933	11.03
	4-4	3.82×10^{-6}	0.988	12.13

In Fig.18, flexural strength at high temperatures is shown for the material with 4-4w/o additives. Strength degradation can be observed above $\approx 800^\circ\text{C}$, which attributed to softening of glass phase existing in grain boundaries at high temperatures.

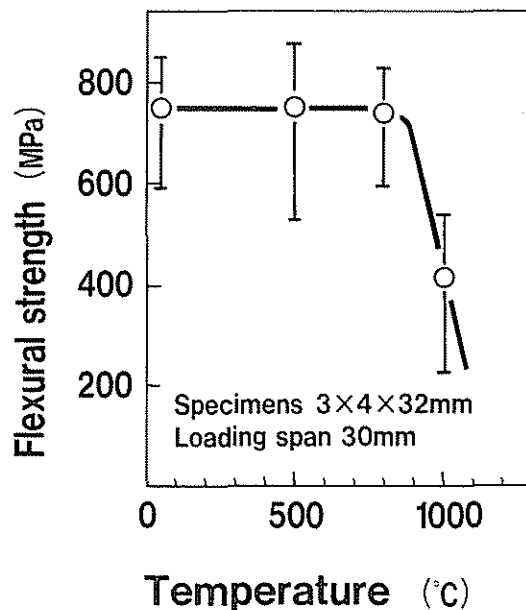


Fig.18 - Flexural strength at high temperature

Fracture toughness was measured by vickers indentation method developed by A.G. Evans et al. (1) and G.R. Anstis et al. (2). Figure 19 shows dependence of fracture toughness on temperature in the range up to 800°C in air. The defect size was estimated by plotting $(K_{Ic}/\sigma_{3b})^2$ versus defect size C as shown in Fig.20. Defect size was nearly $40 \mu\text{m}$ at the most, and the size was consistent with that of observed pore at fracture surface as shown in Fig.21.

It is important to know strength degradation after exposure at high temperatures since engine components are used under severe conditions. There was no significant change in flexural strength after annealing of several 100hrs at 1000°C in air.

These results all suggest that the material developed in the present work has sufficient mechanical properties in application for the present diesel engines.

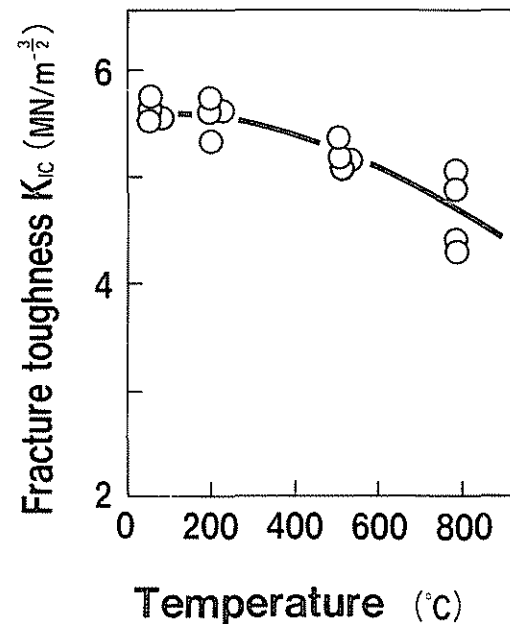


Fig.19 - Dependence of fracture toughness on temperature

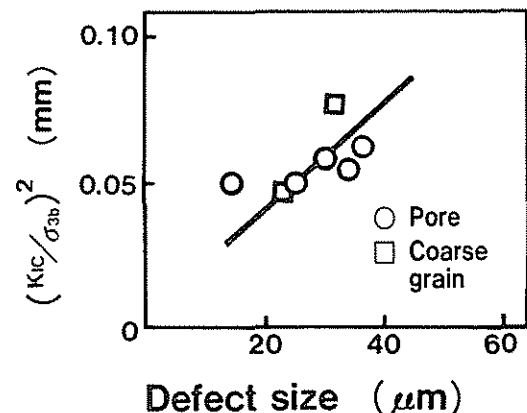


Fig.20 - Correlation between fracture toughness and defect size

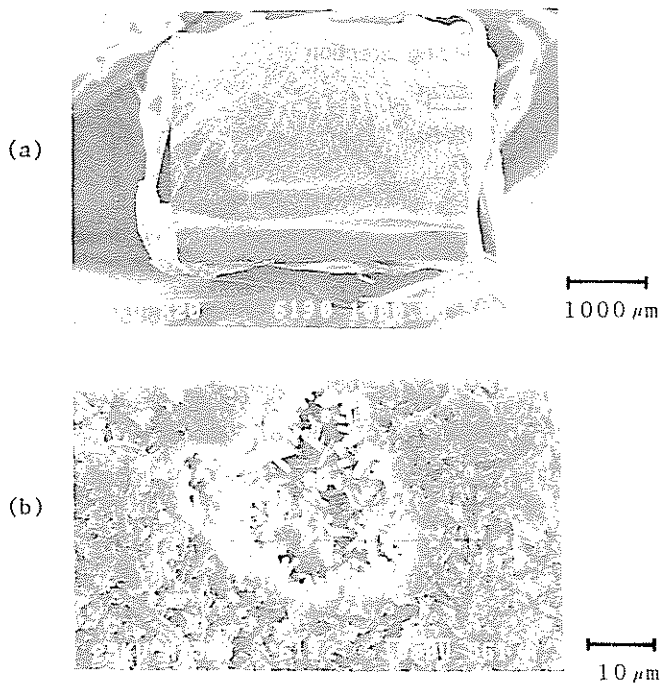


Fig.21 - (a) fracture surface,
(b) fracture origin (pore)

INJECTION MOLDING PROCESS - Ceramic injection molding is suitable for processing complex shaped components with large quantities (3). This method is composed of following process steps, and total processing control is essential to succeed in this method, as each one influences subsequent step.

- (I) Mixing to obtain homogeneous mixture composed of organic binders and ceramic powders
- (II) Injection molding
- (III) Binder removal
- (IV) Sintering

In this work, polypropylene based thermo-plastic binders were used as well as minor plasticizer and additives. The mixing of binders with ceramic powders is important to obtain sufficient flow or viscosity suitable for subsequent molding. The flow characteristics for the mixture can be evaluated by its torque which is measured using high-shearing apparatus. Figure 22 shows flow characteristics for the mixtures prepared by various conditions. The torque indicates rather low value and is proportional to the viscosity above melting point of binders, when homogeneous mixing is attained. This data is useful to determine the final mixing conditions including ceramic powder characteristics.

One of the examples for defects generated by ceramic injection molding is "weld line" which is caused by inadequate adhesion at the front of flow or entrapped air. This type of defect can be eliminated by consideration of injection pressure, injection rate, and hold time.

Binder removal was conducted by heat

treatment of as-molded body utilizing thermal decomposition. Figure 23 shows the weight loss during heat treatment of the sample with heating rate of 10°C/hr . Rapid thermal decomposition can be observed above $\approx 350^{\circ}\text{C}$. The suitable heating pattern was determined based upon above data. Heating rate must be slow enough to prevent cracking and blistering of the body after binder removal.

The suitable sintering conditions including temperature, hold time, and heating rate are different between testing bars with simple shape and complex shaped components. Therefore, final condition was determined by the result on the component itself.

The strength of the swirl chamber fabricated by injection molding was measured using testing bars cut from the sintered body. Strength distribution along axial direction is shown in Fig.24, where strength variations is quite small and Weibull parameter attains 20.3. This suggests that injection molded body is quite homogeneous in the present work.

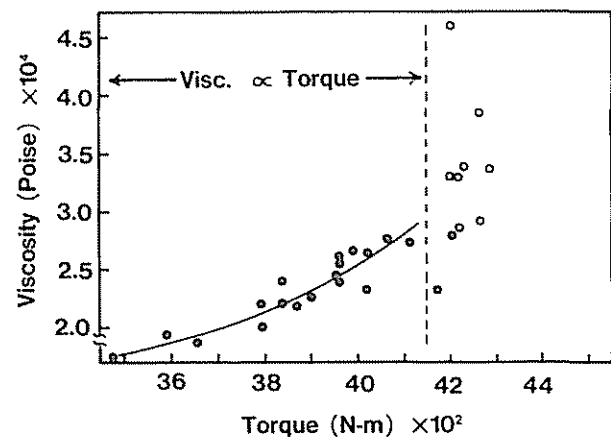


Fig.22 - Torque and viscosity for mixtures

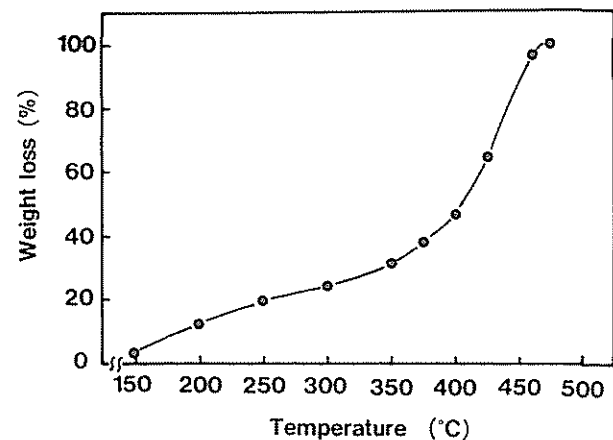


Fig.23 - Weight loss during heat treatment of mixture

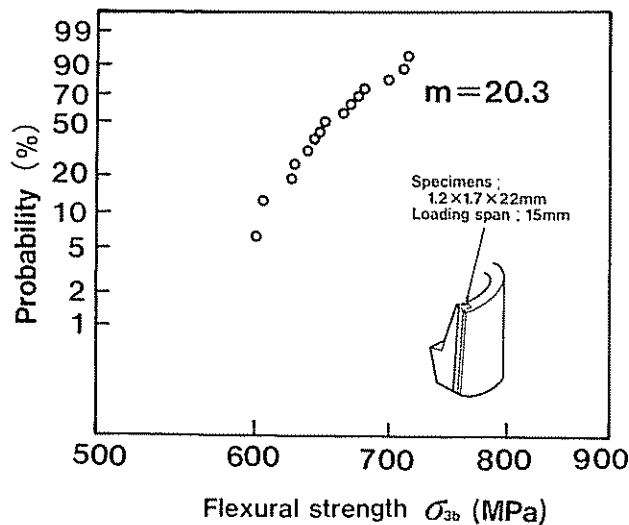


Fig.24 - Flexural strength in axial direction of swirl chamber

MACHINING PROCESS - As sintered swirl chamber is ground at the upper and lower surface as well as the external surface to ensure good tolerance in final size. The grinding of the external surface of the chamber is important, since the maximum stress is applied to the external surface along cylindrical direction as discussed before. It is known that the grinding direction influences the strength of ceramic materials (4). Figure 25 shows that the strength of testing bars with tensile stress normal to the grinding direction can be about 20% lower than those with tensile stress parallel to the grinding direction. It is desirable that the ceramic chamber is ground with conventional cylindrical grinding, as stress is applied along cylindrical direction. In the present work, infeed centerless machining was adopted in consideration of productivity, grinding allowances, cycle time, the numbers of machine, and the size of a diamond wheel. The oscillation method was employed to avoid uneven wheel wear during grinding process.

The objective of the present development is to raise productivity as well as to reduce machining cost. Machining conditions must be determined so as to increase in grinding ratio and to extend dressing interval, because diamond wheel wear directly influences grinding cost for the ceramic chamber. Wheel wear is well known to be affected by stock removal rate (5). However, there is few data on correlation between stock removal rate and grinding ratio in ceramic infeed centerless machining.

It can be recognized that rapid decrease in grinding ratio occurs as stock removal rate becomes larger than a certain value as shown in Fig.26. Figure 27 indicates that grinding force is also increased rapidly above the same stock removal rate as in Fig.26. These suggest that grinding condition changes at this value of the

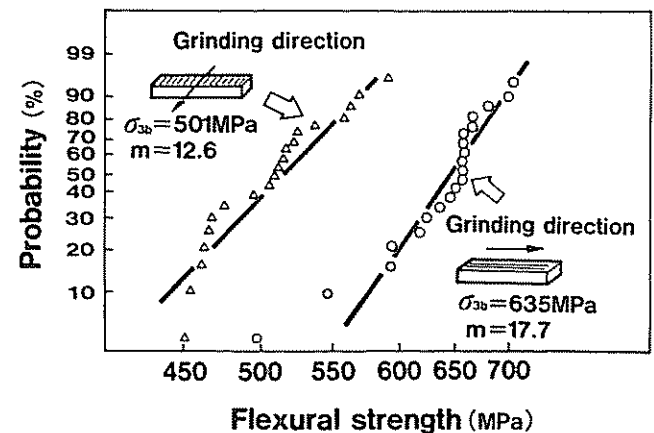


Fig.25 - Flexural strength according to grinding direction

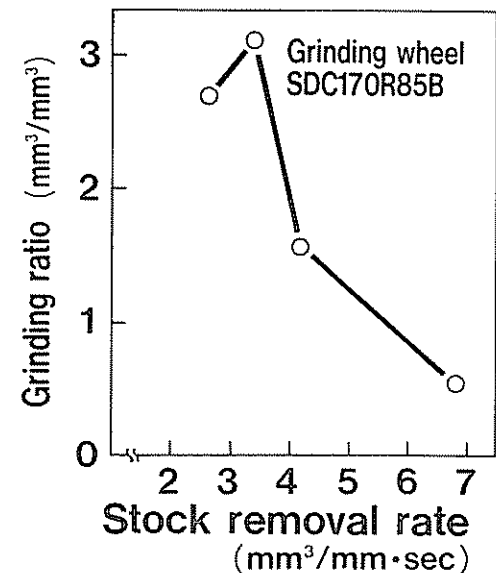


Fig.26 - Stock removal rate and grinding ratio

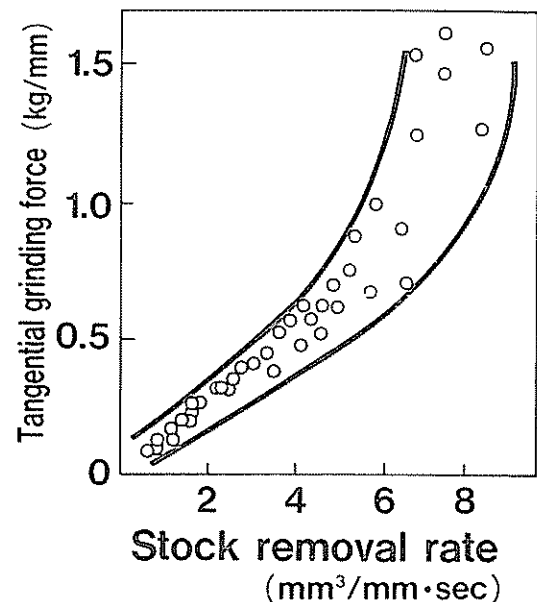


Fig.27 - Stock removal rate and tangential grinding force

stock removal rate. In fact, it can be observed that grain release is much progressed in the case of occurrence of rapid increase in grinding force. Hence, stock removal rate has to be lowered so as to prevent rapid increase in grinding force.

Dressing interval is extended when the grinding is conducted under the condition where grain release and regeneration is stable. The frequent dressing must be avoided, since it is equivalent to grinding wheel wear. The correlation between the number of grains and cumulative stock removal is shown in Fig.28. This data can be obtained by counting the grains in transferred surface of grinding wheel. One of the examples for the transferred surface is shown in Fig.29. The existence of grinding conditions was confirmed where the grain release and regeneration occurred at constant rate from Fig.28. It was possible to make dressing interval extend by determination of grinding condition from these results. Present grinding conditions make it possible to assure the component quality and to reduce machining cost.

The final conditions are summarized in Table 2.

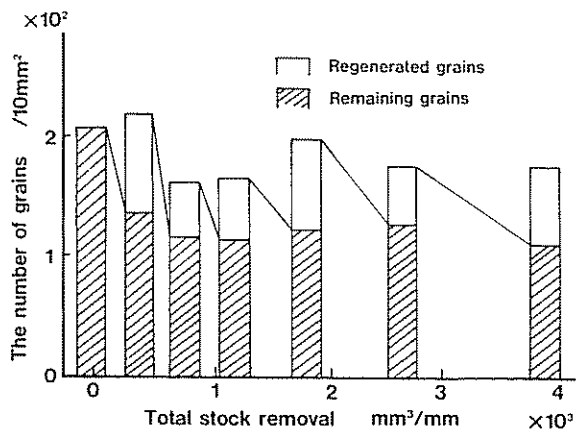


Fig.28 - The numbers of grains in diamond wheel surface

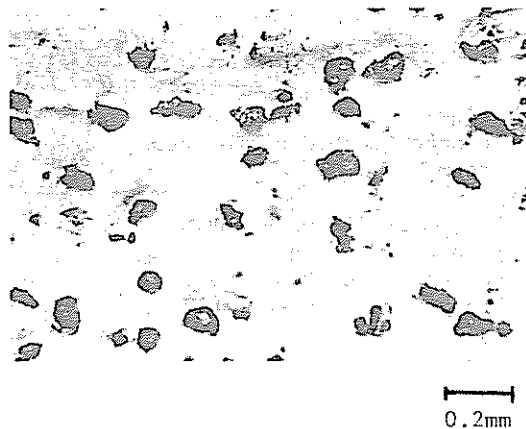


Fig.29 - Transferred surface of wheel after machining process

Table 2 - Machining condition for ceramic swirl chamber

GRINDING WHEEL	SDC17085B
REGULATING WHEEL	A120R3R
GRINDING WHEEL SPEED	1800m/min
REGULATING WHEEL SPEED	12m/min
OSCILLATION SPEED	840mm/min
INFEE RATE	1.0mm/min

INSPECTION METHODS

It is necessary to screen the ceramic chambers since sintered silicon nitride has large strength variations as compared to metallic materials. Several non-destructive inspections were employed which include X-ray radiography, fluorescent penetrant and ultrasonic inspections. Internal flaws more than $\approx 200 \mu\text{m}$ can be detected by X-ray radiography, and fluorescent penetrant inspection is useful for sharp flaws existing in all the surface of the component. Ultrasonic can detect internal defects with the size above $\approx 50 \mu\text{m}$, and external defects above $\approx 100 \mu\text{m}$ in the present work (6).

However, these non-destructive inspections can't ensure all the regions in the swirl chamber because the failures of the chamber occurred after durability testing from the regions in which above inspections could detect no defects. Therefore, the regions applied higher stresses can be ensured by thermal-stress loading and mechanical-stress loading inspections. Thermal stress loading was conducted by heat-treatment for inner surface of the chamber using propane burner, which generated stresses higher than in engine operation. Mechanical-stress loading was performed by application of inner pressure to the swirl chamber.

Quality assurance for all the chambers has been made by these inspections in the present work.

RELIABILITY EVALUATION METHODS

LONG TERM DURABILITY OF THE SWIRL CHAMBER - It is essential to assure component reliability, particularly in the case of ceramic material for engine parts. For example, it is said that life prediction for ceramic materials can be made by following equation using stress intensity factor, crack propagation rate and Weibull probability theory (7).

$$\ell_n L = \ell_n \left[\frac{2 \{ \ell_n (1-P) - 1 \}^{\frac{m-2}{m}}}{A \sigma^n Y^2 (n-2) K_{IC}^{\frac{n}{m-2}}} \right] + \frac{(n-2) B}{m}$$

L;life, n;crack propagation parameter,
m;Weibull parameter, σ ;applied stress,
P;probability, K_{IC} ;fracture toughness,
A,B;constant, Y;shape parameter

However, as engine components are subject to various loading history, it is not sufficient to assure strength of the component on the supposition of a single axial stress as in above equation. Hence, several reliability testings were performed as follows.

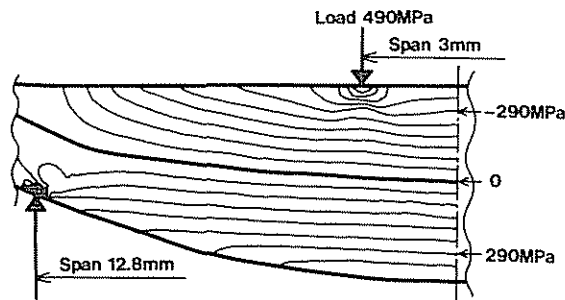


Fig.30 - FEM stress distribution for circular shaped specimen

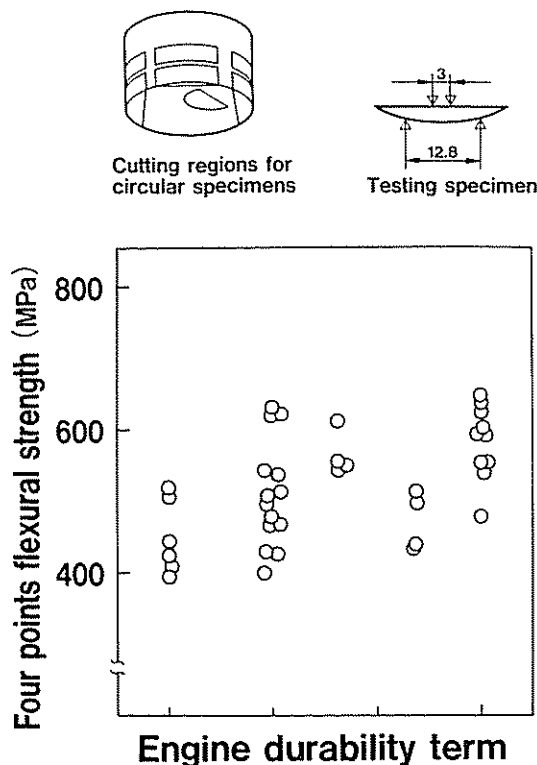


Fig.31 - Flexural strength in lower out side in swirl chamber according to engine durability term

The component strength was measured by circular shape specimens cut from the component along cylindrical direction. FEM analysis and strain measurement confirmed that strength of these specimens could be evaluated within a few percents of experimental errors as compared to rectangular shaped specimens (Fig.30). The flexural strength for circular specimens is shown in Fig.31 according to engine durability term. The strength for upper region of the component was also evaluated using ring shaped specimens which were subject to tensile stress loaded by inner pressure as shown in Fig.32. It seems that there is no slow crack growth since strength degradation can't be detected after engine durability testing as shown in Fig.31 and Fig.32. The estimation for the strength of the component itself from that of small specimens can be made by effective volume method based on Weibull probability theory (8).

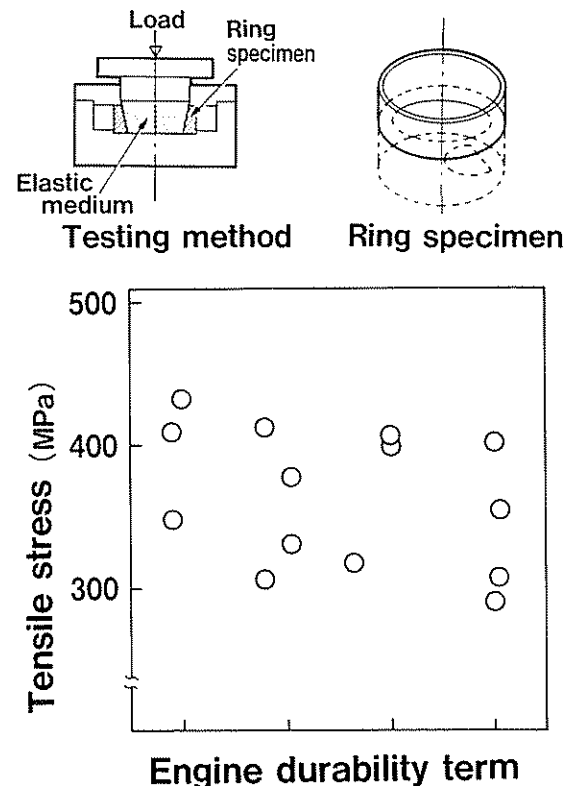


Fig.32 - Tensile strength in upper region in swirl chamber according to engine durability term

INFLUENCE OF PISTON STAMPING - It is necessary to evaluate the strength and durability for the component under severe environment, as engine component must be durable under various conditions. One of the examples is the influence of piston stamping. The large compressive loading may be applied to the chamber, if excess deposit can be generated between bottom surface of the chamber and top end of the piston head. The compressive strength of the chamber is summarized in Table 3. High compressive strength





850523

11

for the chamber is apparent independent of deposit material and compressive position. Figure 33 shows the result for stamping load by piston head, where deposit was attached intentionally in bottom surface of the chamber, and stamping load was estimated by measured strains under engine operation.

These results show that compressive strength of the chamber is more than 10 times of excess loading from piston head.

Table 3 - Compressive strength of swirl chamber

Deposit Hardness Compressive position	Aluminum Alloy Hv83	Aluminum H _v 44	Graphite H _v 257
	56800	—	>29000
	130000	—	>107800
	—	33700	—
	—	26000	—

(Unit, N)

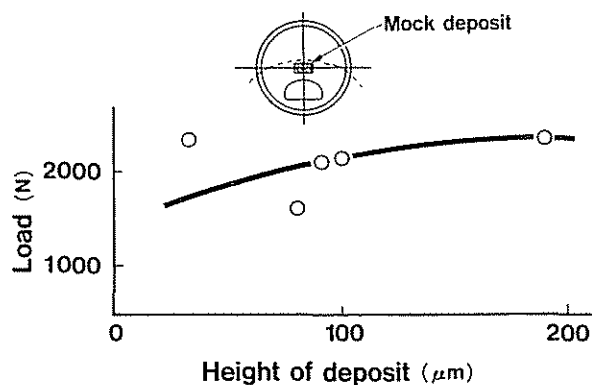


Fig.33 - Stamping load by piston head

ENGINE PERFORMANCE

The adjustment of engine performance was made in consideration of compression ratio, boost pressure, injection timing and injection quantity in order to utilize ceramic capabilities at high temperatures. Power out put can be increased according to an increase in temperature of the combustion chamber as shown in Fig.34. In these steps, the injection quantity and injection

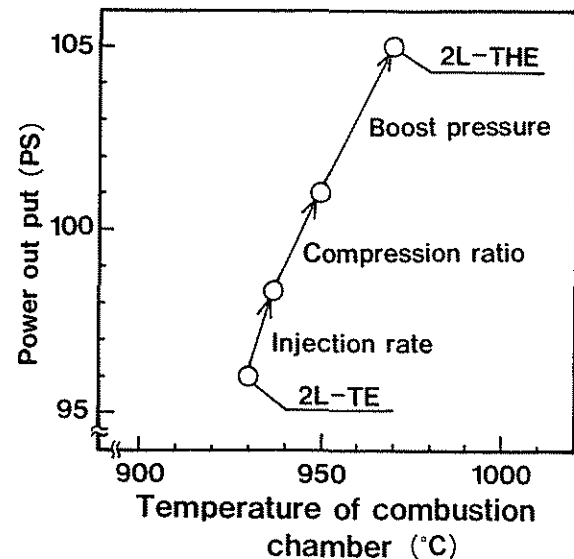


Fig.34 - Engine performance in power out put

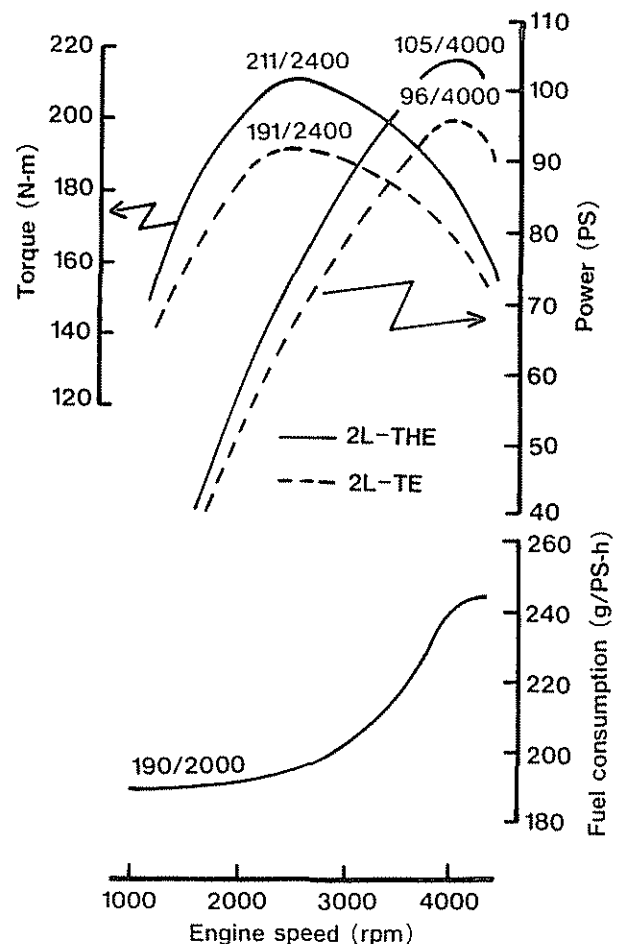


Fig.35 - Comparison of engine performance

Table 4 - Comparison of major specifications

Engine	2L-TE	2L-THE
Numbers of Cylinder	4	←
Bore x Stroke (mm)	ø92 x 92	←
Displacement (cm ³)	2446	←
Valve Mechanism	OHC, Timing Belt Drive	←
Type of Combustion Chamber	Swirl Chamber	←
Compression Ratio	20.0	21.0
Injection Pump	Bosch VE Distributor-type	←
Injection Quantity at Maximum Power (mm ³ /st)	52	57
Maximum Power (PS/rpm), JIS gross	96/4000	105/4000
Maximum Torque (N.m/rpm), JIS gross	191/2400	211/2400
Boost Pressure (mmHg)	350	400
Nozzle Opening Pressure (MPa)	11.8	15.7

timing were adjusted to compression ratio, boost pressure, and injection rate in order to obtain maximum power performance. The upper limit for these parameters was determined by the limitation of smoke concentration, exhaust gas emissions and temperature.

Conventional metallic chamber is employed in 2L-TE, and ceramic chamber is in 2L-THE engine. Comparison of major specifications and engine performance are shown in Table 4 and Fig.35, respectively. The increase in engine performance is apparent in wide range of engine speeds and the maximum power output can be increased from 96 to 105 PS by application of silicon nitride swirl chamber. In addition, there was no significant change in engine efficiency or emissions for the 2L-THE engine with ceramic chamber as compared to 2L-TE engine.

SUMMARY

Sintered silicon nitride swirl lower-chamber has been developed in order to improve performance of turbocharged diesel engines. The results obtained in this work are

summarized as follows.

- (1) Design specifications for the ceramic chamber have been determined by FEM analysis and stress measurements for thermal stress, combustion stress and assembly fixing forces.
- (2) Sintered silicon nitride has average flexural strength of more than 700 MPa with Y₂O₃ and MgAl₂O₄ as oxide additives, and ceramic injection molding has employed to fabricate the swirl chambers with large quantities.
- (3) Quality assurance and cost reduction in machining process can be attained by infeed centerless method and selection of machining conditions suitable for ceramic materials.
- (4) Reliability of the final products was assured by reliability evaluation methods as well as non-destructive and stress loading inspections.
- (5) Power performance of turbocharged diesel engine with ceramic chamber has been increased in 9 PS (7KW) as compared to that of conventional engine by adjusting injection rate, compression ratio and boost pressure.

ACKNOWLEDGEMENTS

Authors are grateful to Dr. O. Kamigaito and co-workers in Toyota Central Research and Development Laboratory Incorporation for their valuable discussions and offer of some datum.

REFERENCES

- (1) A.G. Evans and E.A. Charles, "Fracture toughness determinations by indentation", J. Am. Ceram. Soc., 59(1976)371.
- (2) G.R. Anstis, P. Chantikul, B.R. Lawn and D.B. Marshall, "A critical evaluation of indentation techniques for measuring fracture toughness: I, Direct crack measurements", J. Am. Ceram. Soc., 64(1981) 533.
- (3) B.C. Mutsuddy, "Injection molding research paves way to ceramic engine parts", Ind. R & D. July(1983)76.
- (4) C.A. Andersson, R.J. Bratton, "Effect of surface finish on the strength of hot pressed silicon nitride", N. B. S. Special Publication 562(1979)463.
- (5) T. Nakajima, Y. Uno, and H. Yoshinobu, "Cylindrical plunge grinding of fine ceramics", J. Ja. Soc. Prec. Eng., 50, N04 (1984)
- (6) K. Asai, A. Takeuchi, and N. Ueda, "Computerized ultrasonic inspection system for ceramic precombustion chambers of automotive diesel engines", to be presented in this congress. (1985)
- (7) A.G. Evans and S.M. Wiederhorn, "Proof testing of ceramic materials-an analytical basis for failure prediction", Intl. Jnl. Frac., 10(1974)379.
- (8) D.G.S. Davies, "The statistical approach to engineering design in ceramics", Proc. Brit Ceram. Soc., 22(1973)429.

This paper is subject to revision. Statements and opinions advanced in papers or discussion are the author's and are his responsibility, not SAE's; however, the paper has been edited by SAE for uniform styling and format. Discussion will be printed with the paper if it is published in SAE Transactions. For permission to publish this paper in full or in part, contact the SAE Publications Division.

Persons wishing to submit papers to be considered for presentation or publication through SAE should send the manuscript or a 300 word abstract of a proposed manuscript to: Secretary, Engineering Activity Board, SAE.

Printed in U.S.A.